

Modified KCl Molten Salt Method Synthesis of Spinel $\text{LiNi}_{0.5}\text{Mn}_{1.5}\text{O}_4$ with Loose Structure as Cathodes for Li-ion Batteries

Xu Lu, Xiuqing Lin, Yesheng Shang, Tao Huang, Aishui Yu*

Department of Chemistry, Collaborative Innovation Center of Chemistry for Energy Materials, Shanghai Key Laboratory of Molecular Catalysis and Innovative Materials, Institute of New Energy Fudan University, Shanghai 200438, China

*E-mail: asyu@fudan.edu.cn

Received: 25 August 2014 / Accepted: 18 September 2014 / Published: 29 September 2014

Spinel $\text{LiNi}_{0.5}\text{Mn}_{1.5}\text{O}_4$ (LNMO) with a loose structure is successfully synthesized through a modified KCl molten salt method for the first time. Firstly, the precursor is prepared by a sol-gel method, and then it is calcined with LiOH and the KCl molten salt to synthesize the product. To evaluate the effect of the synthesis conditions on the formation of spinel LNMO, the molten salt and calcination atmosphere are investigated in detail. The structure and morphology of the materials are characterized by X-ray diffraction and scanning electron microscopy. The LNMO synthesized under optimized condition exhibits a loose morphology consisting of 500-800 nm particles and more excellent electrochemical performance especially in the rate performance, receiving a discharge capacity of 108.3 mAh g^{-1} at 10 C. The superior performance is attributed to both the loose structure and uniform particle.

Keywords: Cathode; Spinel; Li-ion battery; High-voltage; molten salt; sol-gel process

1. INTRODUCTION

The huge demands for high-power application have motivated the development of battery materials [1-3]. One of the most promising candidates is the spinel-like $\text{LiNi}_{0.5}\text{Mn}_{1.5}\text{O}_4$ (LNMO), considering its lower toxicity, lower cost, and higher theoretic capacity [4-8]. Compared to the traditional cathode material LiMn_2O_4 , LNMO exhibits improved structural stability because of the absence of Mn^{3+} . This material also has a two-electron transition from Ni^{2+} to Ni^{4+} with two voltage plateaus near 4.7 V vs. Li^+/Li , fast three-dimensional lithium-ion diffusion paths within the cubic lattice and a theoretical capacity of 147 mAh g^{-1} [9-12].

However, the rate performance and the cyclic performance at a high current density of LNMO are facing serious challenges. To solve these problems, considerable research has been focused on its physical properties, particularly its particle size, particle morphology, crystal structure and Mn^{3+} content. Zhang et al. reported a morphology-inheritance route to prepare 1D nanoporous LNMO and the materials delivered an outstanding rate performance [13]. Liu et al. synthesized LNMO cathode materials through a two-step approach, which exhibited excellent performance, high capacity and good cyclic stability [14].

In general, LNMO is always synthesized by a solid-state method [15, 16]. However, solid-state procedure produces larger particles with poor control of their stoichiometry and shape. Some disadvantages of the conventional solid-state method could be eliminated or minimized by a sol-gel method. B.J. Hwang et al. synthesized the spinel $\text{Li}_{1.02}\text{Ni}_{0.5}\text{Mn}_{1.5}\text{O}_4$ by a citric acid-assisted sol-gel process followed by sintering under O_2 flowing conditions [17]. In addition, the molten-salt method is another route to synthesize LNMO, and it has been reported as the simplest method for preparing ceramic materials [18]. The molten salt method is based on the application of a salt with a low melting point. In the molten salt, diffusion rates between reaction materials are much higher, thus powders with a single phase can be obtained at a lower temperature. Previous studies reported that the LNMO could be synthesized only in a covered crucible in a LiCl flux and the synthesis in the open state would lead to the formation of the Li_2MnO_3 impurity because of the excessive Li^+ [19].

In this paper, the KCl molten salt was used in the synthesis of LNMO for the first time to avoid the Li_2MnO_3 impurity and the LNMO powders were obtained in the open state. Furthermore, the molten salt successfully maintained the loose structure of the precursor prepared by a sol-gel method. The LNMO powders were synthesized by the calcination of a mixture of the precursor, LiOH and the KCl molten salt. The influence of molten salt and sintering atmospheres were discussed in detail. The materials synthesized under optimized condition show excellent electrochemistry performance.

2. EXPERIMENTAL

2.1. Preparation and characterization

2.1.1. Preparation of LNMO materials

The LNMO powders were synthesized by a modified KCl molten salt method. Stoichiometric amounts of $\text{Mn}(\text{CH}_3\text{COO})_2 \cdot 4\text{H}_2\text{O}$, $\text{Ni}(\text{CH}_3\text{COO})_2 \cdot 4\text{H}_2\text{O}$ and citric acid were dissolved in distilled water and stirred continuously. The mole ratio of citric acid to total metal ions was 1. After adjusting the pH value to 7.0-8.0 with ammonium hydroxide, the solution was evaporated at 80 °C at 400 r/min until a green gel formed. The gel was dried in a vacuum oven at 120 °C for 15h. The obtained powders were decomposed at 500°C for 6 h. The precursor powders were ground with a appropriate amount of LiOH and a large excess of KCl, of which the molar ratio for the precursor was 4 (hereafter, the molar ratio of KCl for the mixed precursors is defined as R). After sufficient mixing, the mixture was placed in an alumina crucible and calcined under different atmosphere where the gas flow consisted of O_2 and

N₂ at O₂ concentrations of 10%, 20%, 50% and 100%. The samples were then calcined at 900 °C for 12 h and then cooled to room temperature naturally. Finally, the resulting powders were washed with distilled water and dried at 120°C.

For the purpose of comparison, the LNMO powders were also synthesized by an ordinary sol-gel method and calcined at 900°C in O₂ flow for 12 h.

2.2. Physical characterization

The structure of the as-prepared powders was confirmed by X-ray diffraction (XRD, Bruker D8 Advance, Cu K α radiation, $\alpha=1.5406$ Å) with a range of 2θ from 10° to 80° at a scan rate of 1°/min. The morphology and composition of the samples were investigated by scanning electron microscopy (SEM, JEOL JSM-6390).

2.3. Electrochemical measurements

The working electrodes were prepared by mixing 80 wt.% as-prepared powders, 10wt.% carbon conductive agents (super P) and 10 wt.% polyvinylidene difluoride (PVDF) binder in N-methyl-2-pyrrolidone (NMP) solvent. The slurry was then cast onto an aluminum foil current collector. After coating, the electrodes were dried at 80 °C for 3h. Then, the electrode film was punched into disks with a typical diameter of 12 mm. The electrodes were dried overnight at 80 °C in a vacuum oven prior to use. A metallic lithium foil was used as an anode, 1 M LiPF₆ in ethylene carbonate (EC) - diethyl carbonate (DEC) (1:1 in volume) was used as the electrolyte, and a polypropylene microporous film (Cellgard2300) served as the separator. Coin-type (CR2032) half-cells were assembled in an argon-filled glove box (Mikarouna, Superstar 1220/750/900). The galvanostatic discharge-charge measurements were performed on a battery test system (Land CT2001A, Wuhan Jinnuo Electronic Co. Ltd.) between 3.5 and 4.9 V (vs. Li⁺/Li) at different rates at room temperature. EIS measurements were performed on an electrochemical workstation (CH Instrument 660A, CHI Company). The amplitude of the AC signal was 5 mV over a frequency range from 100 kHz to 10 mHz.

3. RESULTS AND DISCUSSION

3.1. Effect of synthesis conditions

In this paper, the precursor was prepared by sintering dry gel, and the LNMO powders were synthesized by calcining a mixture of the precursor, LiOH, and the KCl molten salt. To reveal the effect of the KCl molten salt on the sol-gel method precursor, we synthesized spinel LNMO powders from a sol-gel method precursor at different conditions: one was calcined with LiOH and KCl molten salt (R=4) (modified KCl molten salt method) and the other was calcined with LiOH only (sol-gel method). Both samples were calcined at 900 °C for 12h in O₂ flow. Fig. 1 (1) shows the XRD patterns of the two groups of samples. Although all of the diffraction peaks were in good agreement with

JCPDS card 80-2162, the LNMO samples calcined directly (LNMO-SG here after) exhibited $\text{Li}_x\text{Ni}_{1-x}\text{O}$ impurity peaks at 37° and 44° in 2θ .

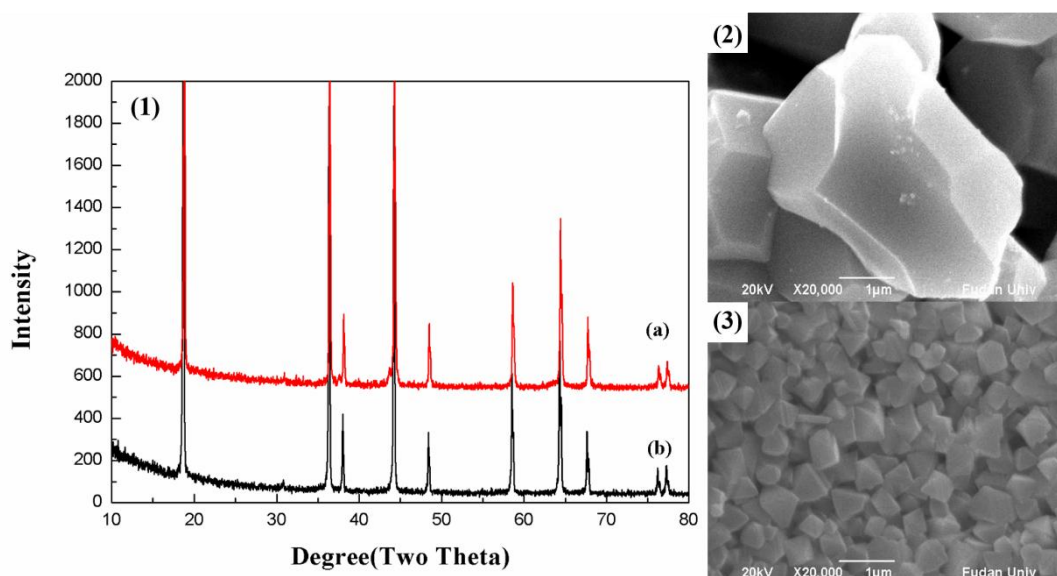


Figure 1. XRD patterns of the (1) LNMO powders synthesized by different methods: (a) the sol-gel method and (b) modified KCl molten salt method. SEM images of the LNMO powders synthesized by different methods: (2) the sol-gel method and (3) molten salt method.

However, these peaks were no longer seen in the samples synthesized by modified KCl molten salt method (LNMO-MS here after) because of the faster phase formation in the molten medium [20]. The XRD of LNMO-MS also shows that the Li_2MnO_3 impurity reported in the LiCl molten salt method was successfully eliminated [19]. The Fig. 1 (2) (3) shows the SEM images of the two groups of samples mentioned above. The LNMO-MS exhibited single crystals of octahedral shape with [111] planes and a characteristic loose morphology, whereas the LNMO-SG particles were irregular, indicating that the LNMO-MS exhibited better crystallinity. The image also shows that the particle size of LNMO-MS is approximately 500-800 nm.

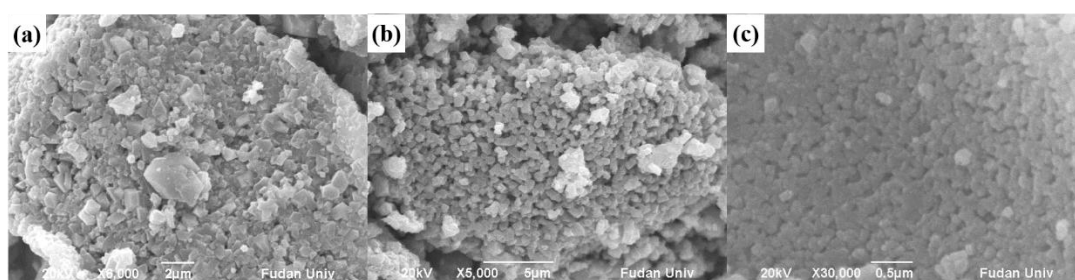


Figure 2. SEM images of the LNMO powders synthesized in different ratios of KCl molten salt: (a) R=1; (b) R=4; (c) R=16.

The morphology of the LNMO samples significantly varied with the change of the molten salt amount. We synthesized three groups of materials in different amounts of KCl molten salt ($R=1, 4, 16$). Fig. 2 (a)–(c) show the SEM images of the samples. As shown in Fig. 2, the particle exhibits bigger size and more significantly aggregation with the decreasing of the KCl molten salt ratio. Fig. 2 (a) represents the sample of $R=1$.

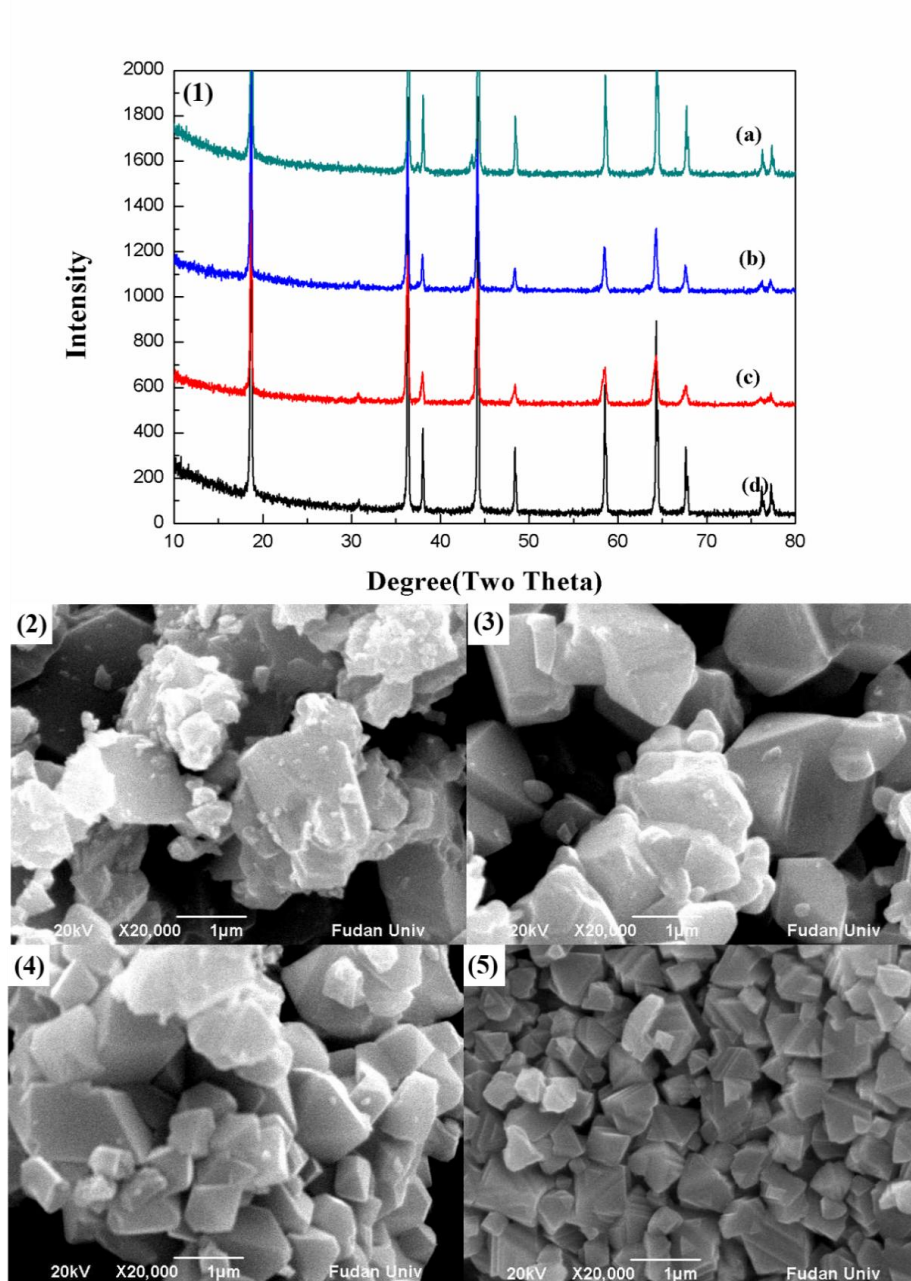


Figure 3. XRD patterns of the (1) LNMO powders synthesized under different atmospheres: (a) 10% O_2 ; (b) 20% O_2 ; (c) 50% O_2 and (d) 100% O_2 . SEM images of the LNMO powders synthesized under different atmospheres: (2) 10% O_2 ; (3) 20% O_2 ; (4) 50% O_2 and (5) 100% O_2 .

The particle size of 1–4 μm and terrible aggregation can be observed because the deficient molten salt cannot pack and isolate the particles well during synthesizing process. Fig. 2 (b) represents

the sample of $R=4$. The better crystallinity and loose structure can be found because of the appropriate amount of molten salt to packing particles. Fig. 2 (c) represents the sample of $R=16$. It is significant that the particle size is only about 100 nm. It is considered that the particles about 100 nm are easy to aggregate after calcination in 900 °C. However, the sample of $R=16$ maintained a loose structure and little aggregation. We attribute the preservation of the loose morphology to the abundant molten salts that packed the particles and prevented them contacting each other during sintering process. The formation process was discussed in the next chapter. Considering the decomposition of electrolyte on the materials surface, we selected KCl molten salt ratio of $R=4$ as the optimality condition.

To investigate the effect of calcination atmosphere, especially the content of O_2 on the preparation of spinel LNMO, we synthesized the samples at different atmospheres where the gas flow consisted of O_2 and N_2 with an O_2 concentration of 10%, 20%, 50% and 100%. These samples were calcined at 900 °C for 12 h using the same amount of KCl ($R=4$). Fig. 3 (1) shows the XRD patterns of the different samples. All of the diffraction peaks were in good agreement with JCPDS card 80-2162. Because no superlattice structure was observed, these samples were assigned to the $Fd3m$ space group of the disordered framework [21]. The sharp diffraction peaks indicated good crystallinity. In this structure, Li ions and O_2 ions are respectively occupied in the tetrahedral 8a sites and 32e sites, and Mn or Ni ions are occupied in the octahedral 16d sites. The $Li_xNi_{1-x}O$ impurity peaks in the XRD patterns of the LNMO synthesized at 10%, 20% and 50% O_2 concentrations were observed close to the (311), (400) and (440) reflection peaks [22, 23], respectively; however, these peaks were not observed in the LNMO synthesized at 100% O_2 concentration.

Fig. 3 (2)-(4) shows the SEM images of the LNMO synthesized at 10%, 20%, 50% and 100% O_2 concentrations. The samples synthesized at low O_2 concentration (10%, 20% and 50% O_2 concentrations) exhibited some irregular particles with particle size of 10-50nm which may be attributed to the impurities and undeveloped crystals. However, the sample calcined at 100% O_2 concentration exhibited particles with better crystallinity and octahedral crystals. It may indicate that the O_2 concentration will influence the formation of the impurity and the crystal. The above samples were all synthesized by calcination of a mixture of the precursor, LiOH and KCl ($R=4$). Because the precursor was prepared by sintering the dry gel at 500 °C, the Mn^{2+} ions from $Mn(CH_3COO)_2 \cdot 4H_2O$ were not completely oxidized to Mn^{4+} , and the Mn ion in the precursor was maintained at a lower valence state. It is considered that O_2 contributes to the oxidation of the Mn ions in lower valence states when the LNMO is synthesized at 900 °C. The LNMO synthesized at low O_2 concentration contained more Mn^{3+} ions because of the absence of the O_2 during calcination. As a result, the $Li_xNi_{1-x}O$ impurities formed. In the case of the 100% O_2 concentration calcination condition, the sufficient O_2 led to fewer Mn^{3+} ions and $Li_xNi_{1-x}O$ impurities. To sum up, the abundant O_2 and the appropriate molten salt lead to the loose morphology consisting of well-crystallized particles.

3.2. Mechanism of the formation of the loose structure of LNMO

In this paper, spinel LNMO powders with loose structures were obtained by a modified KCl molten salt method. Fig. 4 shows the SEM images of LNMO-MS. Spinel LNMO powders with a

uniform particle size, excellent crystallinity, little aggregation and a loose morphology were observed. Fig. 5 shows the formation mechanism of LNMO-MS. In the first step, the precursor was synthesized by a sol-gel method. The dry gel was obtained from the solution of acetate and citric acid, followed by sintering at an appropriate temperature.

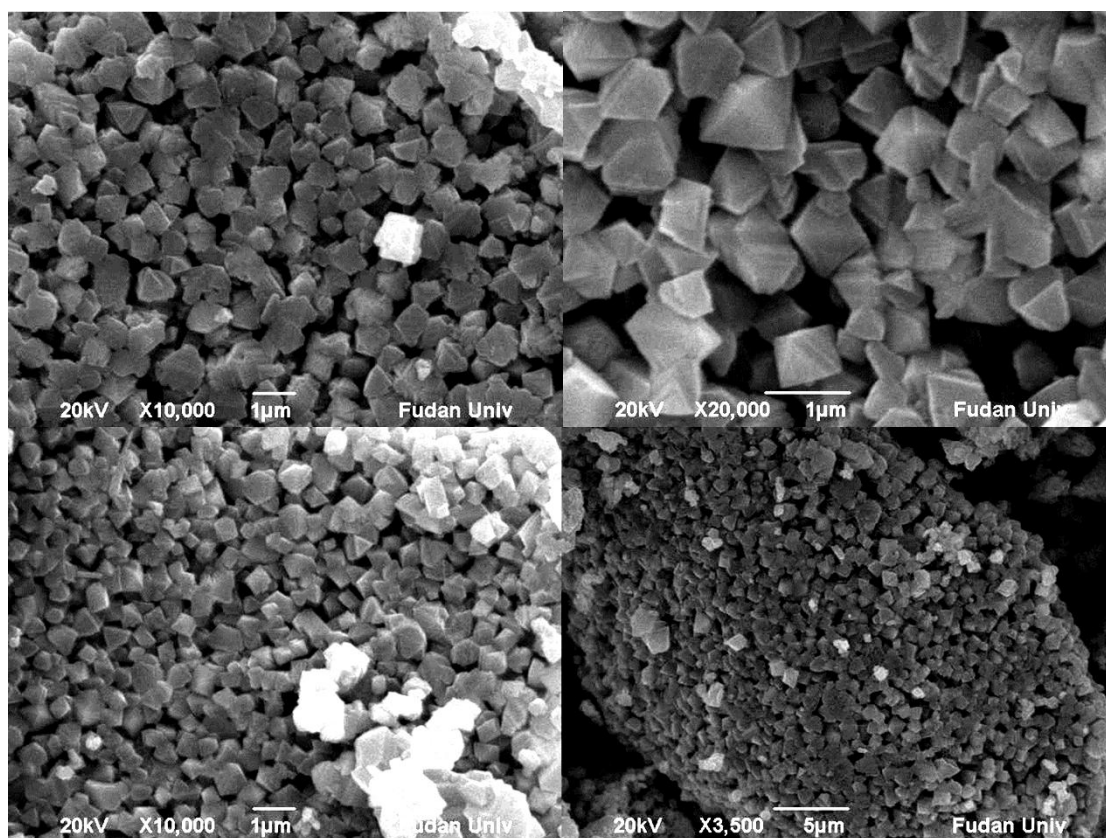


Figure 4. SEM images of the loose structural LNMO powders under different magnifications.

Because of the decomposition of organics, the precursor has a high surface area and loose structure. In the SEM images of the precursor after sintering, the particles of transitional metal oxide with 50-100 nm size could be observed. More importantly, the precursor also reveals a loose morphology, which provides favorable conditions for the molten salt infiltrating and packing the particles in the next step. In the second step, the precursor was calcined and infiltrated with KCl molten salt and LiOH. Referring to Fig. 5, an appropriate amount of KCl led to the packing of the precursor particles, preventing them from contacting each other and maintaining the loose structure. In the third step, the mixture of materials was calcined at a high temperature to synthesize the final product in an O₂ flow. As a result of the facilitation effect of the O₂ flow and the suitable temperature, the spinel LNMO crystalized well resulting in small and uniform particles. Meanwhile, the KCl molten salt between the particles resulted in a loose structure and little aggregation. The SEM image of the LNMO shows the final morphology in which the loose structure and little agglomeration could be observed. This phenomenon indicates that the particles maintained relatively small size and loose

structure and preferred to grow separately rather than aggregate because the KCl molten salt participated in the synthesis process.

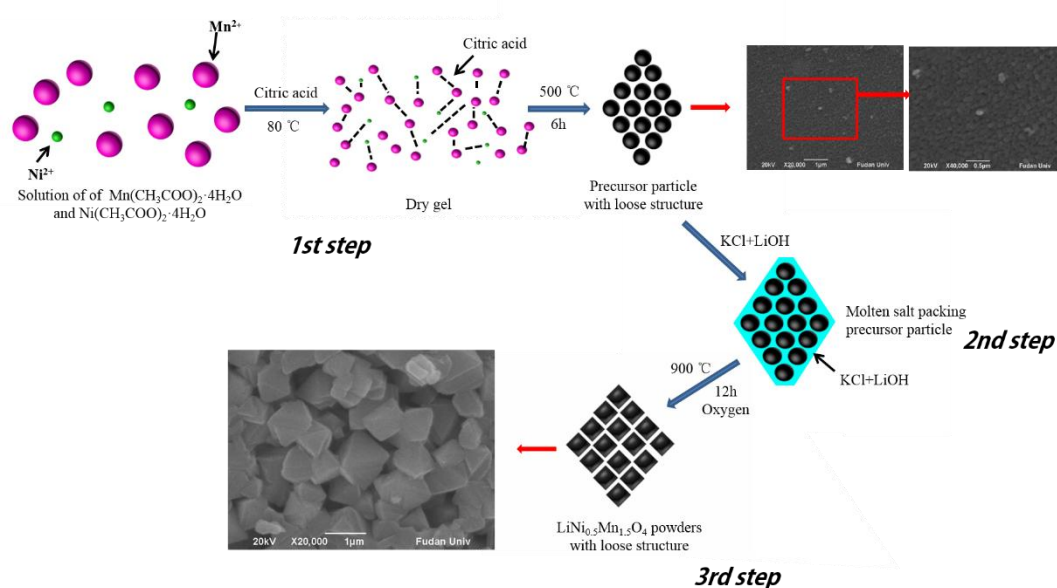


Figure 5. The mechanism of the formation of the loose structural LNMO.

On the basis of the discussion above, we deduce that the KCl molten salt play a role as crystal growth inhibitor. The precursor particles will be packed and isolated well and grow separately in appropriate molten salt. Similarly, the lack of molten salt will lead to the aggregation and bigger particles.

3.3. Electrochemical Characterization

The galvanostatic charge-discharge profiles of LNMO-SG and LNMO-MS at 1 C, 2 C, 5 C and 10 C ($1\text{ C}=140\text{ mA g}^{-1}$) in the potential window of 3.5-4.9 V are shown in Fig. 6. Both groups exhibited a long plateau consisting of two distinct potentials at approximately 4.7V, attributed to the $\text{Ni}^{2+}/\text{Ni}^{3+}$ and $\text{Ni}^{3+}/\text{Ni}^{4+}$ redox couples [21, 24], and a short plateau at approximately 4.0 V, attributed to $\text{Mn}^{3+}/\text{Mn}^{4+}$ because of the Mn^{3+} existing in spinel LNMO [24]. The distinct double-plateau also indicates that both samples exhibited face-centered cubic $Fd\bar{3}m$ (cation disordering) geometry [25, 26]. The shorter plateau at approximately 4.0 V in LNMO-MS indicates fewer Mn^{3+} ions and $\text{Li}_x\text{Ni}_{1-x}\text{O}$ impurities. When the current density ascended up, the plateau of LNMO-SG was influenced more significantly and LNMO-MS has a higher discharge plateau and a lower charge plateau at 4.7V and 4.0V, respectively. Meanwhile, the discharge capacity of LNMO-SG decreased dramatically with the current density increasing. However, the LNMO-MS exhibited much more excellent capacity retention ability. These results indicate that LNMO-MS has a better rate capacity because of its smaller particle size, little polarization, and better crystallinity.

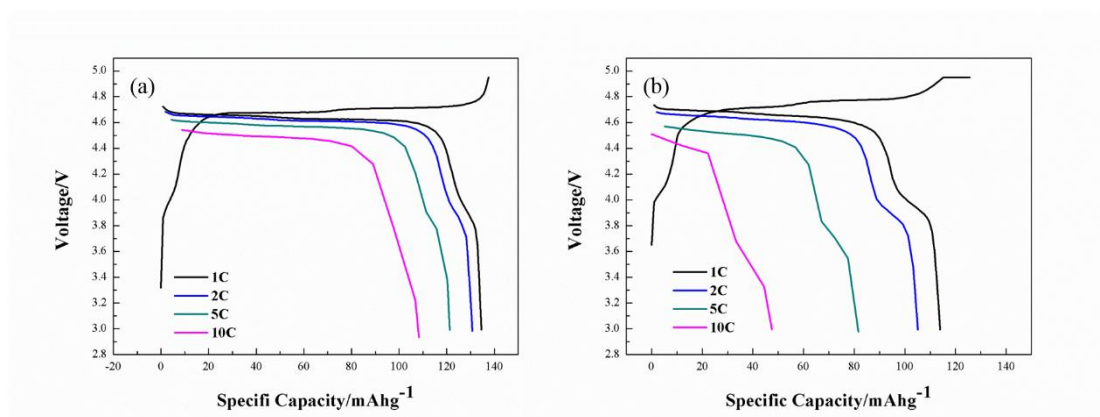


Figure 6. The charge-discharge curves of the LNMO powders synthesized by (a) the modified KCl molten salt method and by (b) the sol-gel method at different current densities.

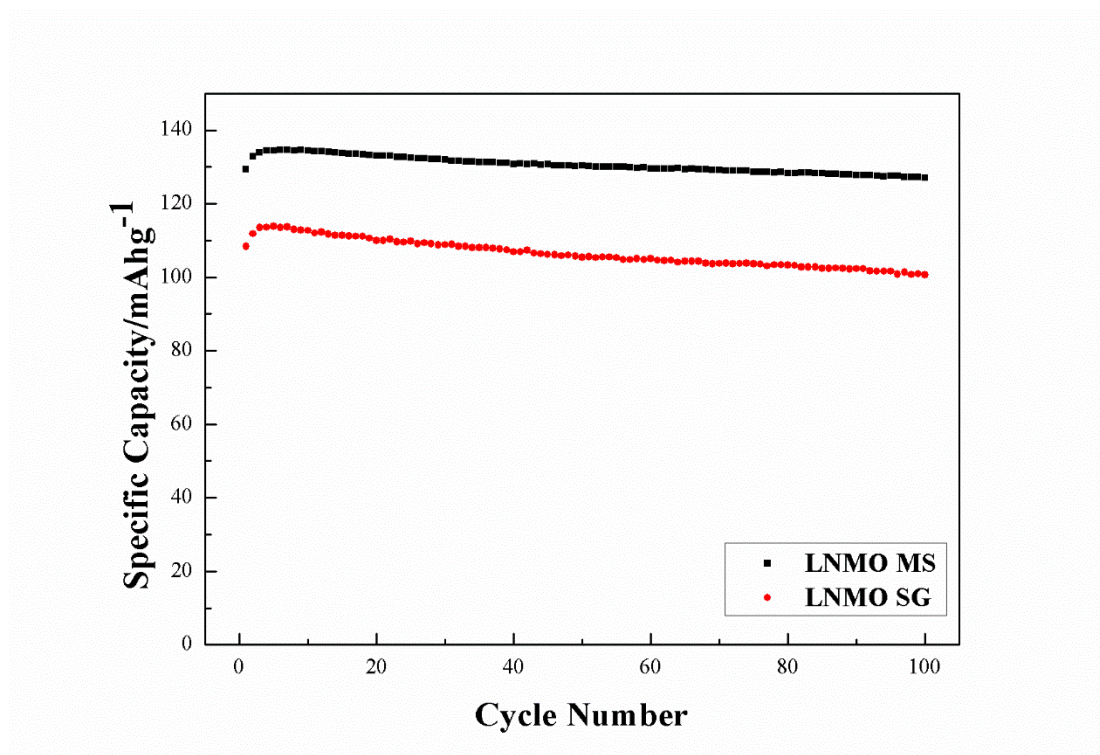


Figure 7. Cycling stability of the LNMO powders synthesized by the modified KCl molten salt method and sol-gel method at 1 C.

The cyclic performance of the two groups of samples was investigated at a high current of 1 C to avoid decomposition of the electrolyte, the results of which are presented in Fig. 7. As shown in the pattern, after a few activating cycles, the discharge capacity of the two groups of samples reached a maximum of 113.9 mAh g⁻¹ for LNMO-SG and 134.6 mAh g⁻¹ for LNMO-MS. After 100 cycles, the discharge capacity of LNMO-SG was only 100.6 mAh g⁻¹, whereas LNMO-MS had a discharge capacity of 127 mAh g⁻¹. The discharge capacity retention rates with respect to the maximum discharge capacity were 88.32% (LNMO-SG) and 94.35% (LNMO-MS). The excellent discharge

capacity retention rate for LNMO-MS was attributed to its high crystallinity and fewer impurities, as demonstrated by the XRD and SEM analyses. The poor cycle performance of LNMO-SG is likely a result of the structural destruction of the undeveloped particle.

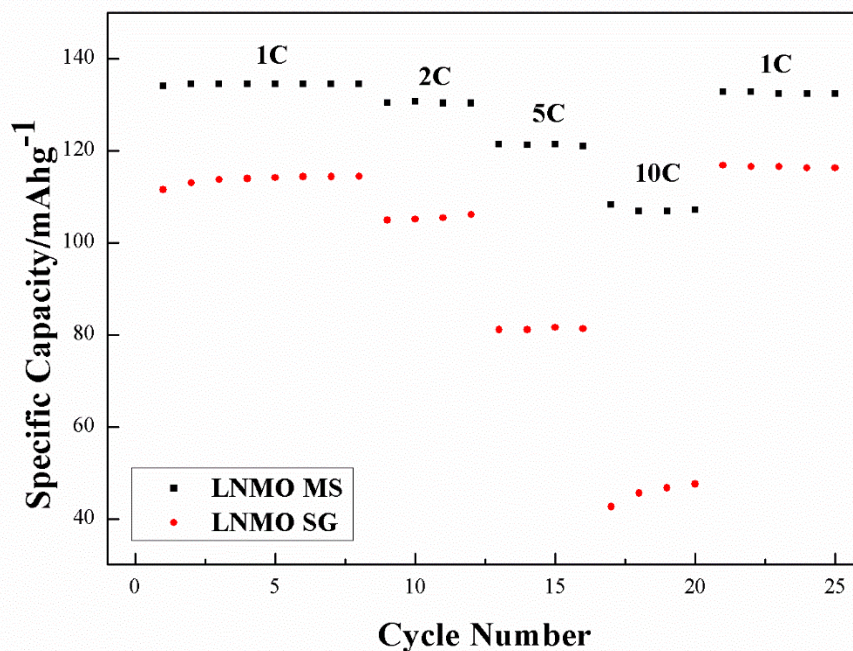


Figure 8. Discharge capacity of the LNMO powders synthesized by the modified KCl molten salt method and the sol-gel method at different current rates.

The rate capacity of both samples was investigated at 1 C, 2 C, 5 C and 10 C. As shown in Fig. 8, the discharge capacities for LNMO-MS were 134.5 mAh g⁻¹, 130.7 mAh g⁻¹, 121.3 mAh g⁻¹, and 108.3 mAh g⁻¹ at the respective current rates listed above. The material also exhibited excellent stability at each current rate with no obvious fading observed. When the current density was reduced back to 1 C, the discharge capacity recovered to its initial value. This result indicates that rapid lithiation/delithiation and a large current density did not result in structural damage of the crystals. The loose structure also led to sufficient infiltration of the electrolyte and the nano-size particle shortened the distances for Li⁺ migration, which allowed the materials to obtain better electrochemical properties. In addition, the material has outstanding cycle performance because of its excellent crystallinity. However, LNMO-SG samples exhibited a poor rate capacity with discharge capacities of 114.4 mAh g⁻¹, 106.1 mAh g⁻¹, 81.6 mAh g⁻¹ and 48.9 mAh g⁻¹ at the respective current densities mentioned above. It is notable that the LNMO-SG sample exhibited low electrochemistry performance (only 48.9 mAh g⁻¹) at a large current density of 10 C. This result indicates that LNMO-SG samples cannot be completely lithiated/delithiated because of electrochemical impedance and polarization. Compared to LNMO-MS, the lower discharge capacity at the same current density for LNMO-SG were attributed to its increased particle size, higher internal resistance and more significant polarization.

To investigate the internal resistance of the samples, EIS patterns for both were performed. Fig. 9 shows the EIS plots of both samples after the 10th, 20th, 30th, and 50th cycle.

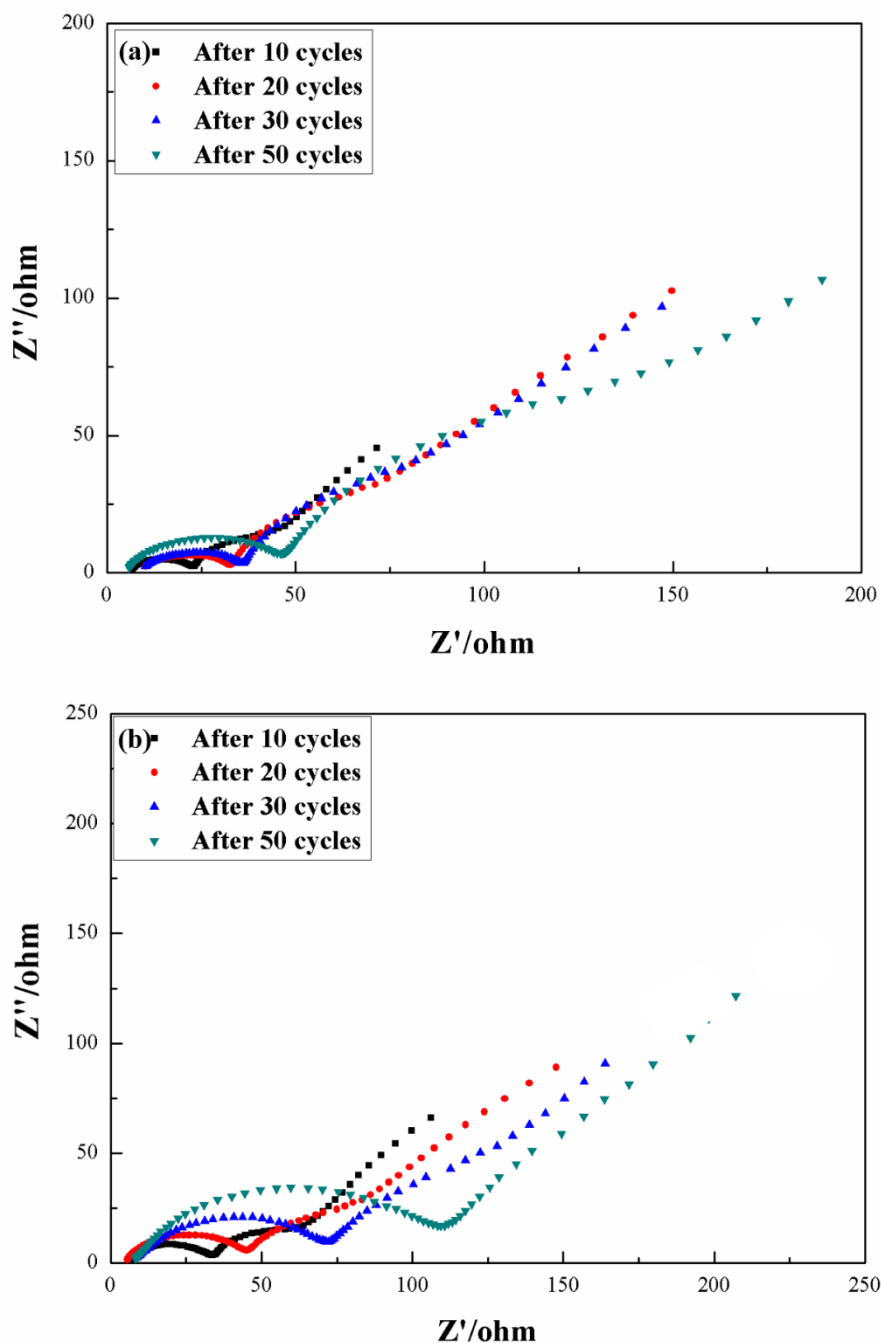


Figure 9. Electrochemical impedance spectroscopy (EIS) of the LNMO powders synthesized by (a) the modified KCl molten salt method and (b) the sol-gel method after different cycles.

Generally, the spectra of both samples are composed of a high-frequency semicircle corresponding to the R_s (the resistance of the surface layer), a medium-to-low-frequency semicircle corresponding to the R_{ct} (charge-discharge resistance at the interface of the electrode and the electrolyte) and the diameter corresponding to the value of R_{ct} . The line at the low-frequency region corresponds to Z_w caused by lithium-ion diffusion in the material [27-29]. Both samples were measured at a potential of 4.5 V. The R_{ct} of LNMO-MS was found to be significantly lower than that of LNMO-SG. This result is possibly attributed to the smaller and more uniform particle size, better

crystallinity with octahedron and the shorter distances for Li^+ migration, as well as the loose structure of LNMO-MS.

4. CONCLUSION

Spinel LNMO was synthesized by a modified KCl molten salt method in which conditions were modified. Among all of the synthesis conditions, the sample synthesized at 900 °C for 12h in O_2 flow with KCl molten salt ($R=4$) exhibited an obviously loose structural morphology with uniform octahedral crystals with a particle size ranging from 500 nm to 800 nm. O_2 facilitated the formation of spinel crystals and the KCl molten salt prevented the aggregation of the particles, both leading to the loose structure. The material also exhibited superior electrochemical performance. The maximum discharge capacity reached 134.6 mAh g^{-1} and the discharge capacity after 100 cycles reached 127 mAh g^{-1} at 1C. Furthermore, an excellent rate capacity was obtained with a discharge capacity of 108.3 mAh g^{-1} at 10 C. We attributed the superior electrochemical properties of these materials to their smaller particle size, high crystallinity and characteristic loose structure.

ACKNOWLEDGEMENTS

The authors acknowledge financial support from 973 Program (2013CB934103) and Science & Technology Commission of Shanghai Municipality (12dz1200402 & 08DZ2270500), China.

References

1. P.G. Bruce, B. Scrosati, J.M. Tarascon, *Angew. Chem. Int. Ed.* 47 (2008) 2930.
2. J. M. Chen, C. H. Hsu, Y. R. Lin, M. H. Hsiao, T. K. Fey, *J. Power Sources* 184 (2008) 498.
3. J.B. Goodenough, Y. Kim, *Chem. Mater.* 22 (2010), 587.
4. Q.M. Zhong, A. Bonakdarpour, M.J. Zhang, Y. Gao, J.R. Dahn, *J. Electrochem. Soc.* 144 (1997) 205.
5. J.G. Li, X.M. He, R.S. Zhao, C.R. Wan, C.Y. Jiang, D.J. Xia, S.C. Zhang, *J. Power Sources* 158 (2006) 524.
6. A. Kraytsberg, Y. Ein-Eli, *Adv. Energy Mater.* 2 (2012) 922.
7. M.H. Zhang, J. Wang, Y.G. Xia, Z.P. Liu, *J. Alloys Compd.* 518 (2012) 68.
8. B. Huang, X.H. Li, Z.X. Wang, H.J. Guo, X.H. Xiong, J.X. Wang, *J. Alloys Comp.* 583 (2014) 313.
9. S. Patoux, L. Daniel, C. Bourbon, H. Lignier, C. Pagano, F. LeCras, S. Jouanneau, S. Martinet, *J. Power Sources* 189 (2009) 344.
10. L. Zhou, D. Zhao, X.D. Lou, *Angew. Chem. Int. Ed.* 51 (2012) 239.
11. S.W. Oh, S.H. Park, J.H. Kim, Y.C. Bae, Y.K. Sun, *J. Power Sources* 157 (2006) 464.
12. G.B. Zhong, Y.Y. Wang, X.J. Zhao, Q.S. Wang, Y. Yu, C.H. Chen, *J. Power Sources* 216 (2012) 368.
13. X.L. Zhang, F.Y. Cheng, J.G. Yang, J. Chen, *Nano lett.* 13(2013) 2822.
14. Z. H. Liu, Y. M. Jiang, X. Y. Zeng, G. Xiao, H. Y. Song, S. J. Liao, *J. Power Sources* 247 (2014) 437.
15. Y. Idemoto, H. Narai, N. Koura, *J. Power Sources* 125 (2003) 119–121.

16. Y.K. Sun, *Solid State Ionics* 100 (1997), 115.
17. B.J. Hwang, Y.W. Wu, M. Venkateswarlu, M.Y. Cheng, R. Santhanam, *J. Power Sources* 193 (2009) 828.
18. R.H. Arendt, *J. Solid State Chem.* 8 (1973) 339.
19. J. H. Kim, S. T. Myung, Y. K. Sun, *Electrochimica Acta* 49 (2004) 219.
20. P. Afanasiev, C. Geantet, *Coord. Chem. Rev.* 178–180 (1998) 1725.
21. K. Ariyoshi, Y. Iwakoshi, N. Nakayama, T. Ohzuku, *J. Electrochem. Soc.* 151 (2004) A296.
22. K. Amine, H. Tukamoto, H. Yasuda, Y. Fujita, *J. Electrochem. Soc.* 143 (1996) 1607.
23. J.H. Kim, S.T. Myung, C.S. Yoon, S.G. Kang, Y.K. Sun, *Chem. Mater.* 16 (2004) 906.
24. Q. Zhong, A. Bonakdarpour, M. Zhang, Y. Gao, J.R. Dahn, *J. Electrochem. Soc.* 144 (1997) 205.
25. M. Kunduraci, G.G. Amatucci, *J. Power Sources* 165 (2007) 359.
26. J.-H. Kim, C.S. Yoon, S.-T. Myung, Jai Prakash, Y.-K. Sun, *Electrochem Solid-State Lett.* 7 (2004) A216.
27. J. Liu, A. Manthiram, *J. Electrochem. Soc.* 156 (2009) A66.
28. H. Duncan, Y. Abu-Lebdeh, I. J. Davidson, *J. Electrochem. Soc.* 157 (2010) A528.
29. E. Barsoukov, J.R. Macdonald, *Impedance Spectroscopy: Theory, Experiment, and Applications*, 2nd ed., Wiley-Interscience, 2005.